JACS Au
AN OPEN ACCESS JOURNAL OF THE AMERICAN CHEMICAL SOCIETY

pubs.acs.org/jacsau
Article

Reactant-Induced Structural Evolution of Pt Catalysts Confined in Zeolite

Xiaoyu Li,† Jinling Cheng,† Huaming Hou,* Debora M. Meira, and Lichen Liu*

Cite This: JACS Au 2024, 4, 666−679
Read Online

ACCESS | Metrics & More | Article Recommendations | Supporting Information

ABSTRACT: Reactant-induced structural evolutions of heterogeneous metal catalysts are frequently observed in numerous catalytic systems, which can be associated with the formation or deactivation of active sites. In this work, we will show the structural transformation of subnanometer Pt clusters in pure-silica MFI zeolite structure in the presence of CO, O_2, and/or H_2O and the catalytic consequences of the Pt-zeolite materials derived from various treatment conditions. By applying the appropriate pretreatment under a reactant atmosphere, we can precisely modulate the size distribution of Pt species spanning from single Pt atoms to small Pt nanoparticles (1−5 nm) in the zeolite matrix, resulting in the desirably active and stable Pt species for CO oxidation. We also show the incorporation of Fe into the zeolite framework greatly promotes the stability of Pt species against undesired sintering under harsh conditions (up to 650 °C in the presence of CO, O_2, and moisture).

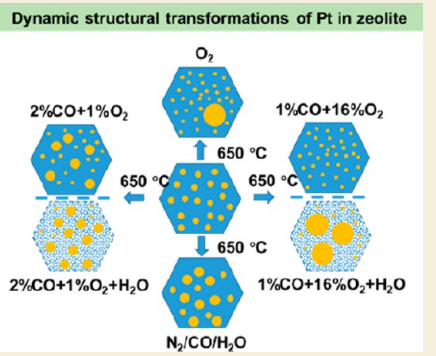

KEYWORDS: *zeolite, platinum, CO oxidation, structural evolution, clusters*

INTRODUCTION

Heterogeneous catalytic processes usually involve the reconstruction of atomic arrangements of the active sites, as demonstrated with studies based on model surface structures and practical catalysts based on nanoparticles.[1,2] The structural evolution of the subnanometer metal species (single metal atoms and metal clusters) on solid carriers under reaction conditions has been commonly observed in numerous supported metal catalysts.[3−5] By following the structural evolution of the metal atoms and clusters, new insights can be obtained in terms of the nature of the active sites, the catalytic mechanism, and the mechanism of catalyst deactivation.[6−9] For instance, single Au atoms transform into subnanometer Au clusters, which serve as the active species for the oxidation of thiophenol to sulfide.[10] However, the continuous sintering of Au clusters into Au nanoparticles leads to catalyst deactivation. In other cases, the exposure of metal particles to the reaction atmosphere will cause the redispersion of metal species and lead to improvements in catalytic performances.[11,12] In this regard, studying the structural evolution of metal species under reaction conditions is not only beneficial for *in situ* generation of highly active sites but also helpful in avoiding the undesired reactant-induced deactivation.[11−16]

Previous studies have shown the dynamic structural evolution of metal catalysts on open-structure solid carriers (e.g., Al_2O_3, TiO_2, and CeO_2) in different atmospheres and metal catalysts confined in zeolites in oxidation−reduction atmospheres.[17−21] However, there is still a lack of systematic and comprehensive study on the dynamic structural evolution of metal species confined in zeolites under reaction conditions. Moreover, due to the profound impacts of moisture on the stability of supported metal catalysts under realistic conditions, it will be of great importance to study the dynamic evolution of zeolite-confined metal catalysts under reaction atmospheres mixed with moisture.[22,23]

In this work, we have followed the structural evolution of subnanometer Pt clusters confined in a crystalline support with regular porous structures (pure-silica MFI zeolite) in different atmospheres and the catalytic consequences of the Pt-zeolite materials derived from various treatments. We can modulate the dispersion of Pt species spanning from single Pt atoms to small Pt nanoparticles (1−5 nm) in the zeolite matrix by tuning the treatment conditions, leading to the formation of a catalyst with high stability against sintering under harsh conditions (up to 650 °C in the presence of CO and moisture) and superior activity for CO oxidation reaction, because of its implications as a classic model reaction in heterogeneous and environmental catalysis.[24,25] The zeolite-encapsulated Pt and bimetallic PtFe catalyst with appropriate size distribution surpass the performance of the well-established Pt/CeO_2 reference catalyst.

Received: November 21, 2023
Revised: January 13, 2024
Accepted: January 16, 2024
Published: February 6, 2024

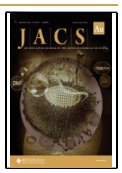

RESULTS AND DISCUSSION

Evolution of Pt-MFI in Different Atmospheres

A Pt-zeolite sample with subnanometer Pt clusters confined in 10MR sinusoidal channels (see Figure S1 and sample preparation details in the Experimental Section) of pure-silica MFI zeolite (named as Pt-MFI) is chosen as a model system because of its regular structure and promising applications in a variety of catalytic reactions.[13,26,27] We will show the evolution behavior of subnanometer Pt species in a crystalline matrix by exposing the Pt-MFI sample to the different atmospheres. First, we tested the stability of Pt clusters in an inert atmosphere at high temperatures. After treatment in N_2 at 450 °C, the particle sizes of the Pt clusters remain stable (Figure 1a and Figure S2). When the treatment temperature is increased to 650 °C, a slight increase in the average particle size is observed (Figure 1b and Figure S3), which should be caused by the thermally driven sintering of Pt clusters. The sizes of the Pt particles continue to increase after treatment in N_2 at 850 °C (Figure 1c and Figure S4), but remain smaller than 2 nm, suggesting the high stability of encapsulated Pt particles in the zeolite matrix.

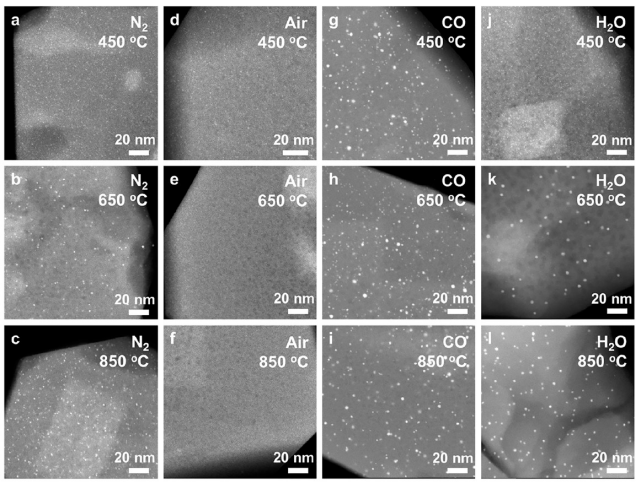

Figure 1. Structural evolution of Pt-MFI in different atmospheres at 450−850 °C. (a−c) HAADF-STEM images of Pt-MFI after treatment in N_2 at 450 °C (a), 650 °C (b), and 850 °C (c). (d−f) HAADF-STEM images of Pt-MFI after treatment in air at (d) 450 °C, (e) 650 °C and (f) 850 °C. (g−i) HAADF-STEM images of Pt-MFI after treatment in 1%CO (balanced by N_2) at (g) 450 °C, (h) 650 °C, and (i) 850 °C. (j−l) HAADF-STEM images of Pt-MFI after treatment in 4%H_2O (balanced by N_2) at (j) 450 °C, (k) 650 °C, and (l) 850 °C.

Then, we treated the Pt-MFI sample with air to check the stability of the Pt species in an oxidative atmosphere. After exposure to air at 450 °C, a large number of subnanometer Pt clusters are preserved (Figure 1d and Figure S5), though the density of the Pt clusters in the zeolite matrix decreases. This phenomenon is more remarkable when the treatment is performed at 650 °C, which nearly leads to the vanishing of the Pt clusters (Figure 1e and Figure S6). It is likely associated with the disintegration of Pt nanoclusters upon exposure to O_2, leading to the formation of PtO_x species.[28] The mobile PtO_x species at high temperatures (e.g., >400 °C) will migrate along the zeolite channels and could be trapped in the defective sites formed by the K-modified silanol nests in the MFI zeolite structure.[13,29] Interestingly, the recovery of Pt clusters can be achieved by subsequent reduction treatment by H_2 at 600 °C (Figure S7), indicating that subnanometer Pt clusters can show reversible transformations between single Pt atoms and clusters in O_2/H_2 atmosphere at 600−650 °C in pure-silica MFI zeolite beyond the reported cases within the silicoaluminate zeolites.[28,30] However, when the calcination treatment is carried at 850 °C, sintering of Pt species into large Pt nanoparticles (>100 nm) is observed (Figure S8), though some atomically dispersed Pt species are still present as indicated by the Pt clusters formed in H_2 atmosphere (Figure 1f and Figures S9 and S10). The XRD peaks corresponding to large Pt particles confirm the severe agglomeration of Pt (Figure S11), inferring that the interaction between PtO_x species and the MFI zeolite is not strong enough for trapping atomically dispersed Pt species at 850 °C.

Moreover, we have studied the evolution behavior of Pt in the CO atmosphere because of the involvement of CO in many metal-catalyzed reactions.[31] Aggregation of Pt clusters into Pt nanoparticles of 1−2 nm is observed after they are subjected to a CO atmosphere (1% CO in N_2) at 450 °C (Figure 1g and Figure S12). Interestingly, with the temperature further increased to 650−850 °C, the particle size distributions of Pt species almost remain unchanged (Figure 1h−i and Figures S13 and S14). The sintering process of Pt species in a CO atmosphere may proceed in the following steps: CO-induced disintegration of Pt clusters toward the formation of mobile $Pt(CO)_x$ species, migration of the $Pt(CO)_x$ species along the zeolite channels and deposition of $Pt(CO)_x$ on large Pt particles.[32] The greatly alleviated sintering of Pt species in the CO atmosphere at 650−850 °C could be ascribed to the limited mobility of $Pt(CO)_x$ in the zeolite matrix because of their larger molecular size than PtO_x.

The large discrepancy in mobility between the PtO_x and $Pt(CO)_x$ species has also been identified in the study on the migration of Pt species from Pt/Al_2O_3 to the Pt-free MFI support in CO or O_2 at 650 °C, respectively. The decreased density of Pt nanoparticles in Al_2O_3 support and the encapsulation of Pt in MFI zeolite is observed after treating the physical mixture of Pt/Al_2O_3 and Pt-free MFI zeolite in O_2, confirming the migration of Pt and the trapping of PtO_x within MFI zeolite (Figures S15 and S16). The agglomeration of Pt nanoparticles on Al_2O_3 and the absence of Pt in MFI zeolite after the treatment of Pt/Al_2O_3 and a Pt-free MFI mixture in CO at 650 °C verify the much lower mobility of $Pt(CO)_x$ in MFI zeolite (Figures S17 and S18).

The stability of metal catalysts under hydrothermal conditions is a critical issue for practical applications in numerous processes.[33,34] The sizes of the Pt clusters confined in the MFI zeolite remain unchanged at 450 °C after treatment with humid N_2 (4% H_2O in N_2) (Figure 1j and Figure S19). However, after elevating the temperature to 650 °C, a considerable portion of the Pt clusters are transformed into Pt nanoparticles of 1−3 nm and some mesopores are formed due to the hydrolysis of Si−O−Si bonds in the MFI framework, as validated by the argon isotherm adsorption (Figure 1k, Figures S20 and S21 and Table S1).[35,36] The agglomeration of Pt is even more severe at 850 °C (Figure S22), which could be associated with deformation of the MFI zeolite structure (Figure S23). We find that narrower size distributions of Pt particles are obtained in the samples after treatments with H_2O than those obtained after treatments with CO, which could be caused by the weaker Pt−H_2O interaction compared to the Pt-CO interaction. When the balanced gas of

https://doi.org/10.1021/jacsau.3c00732
JACS Au 2024, 4, 666−679

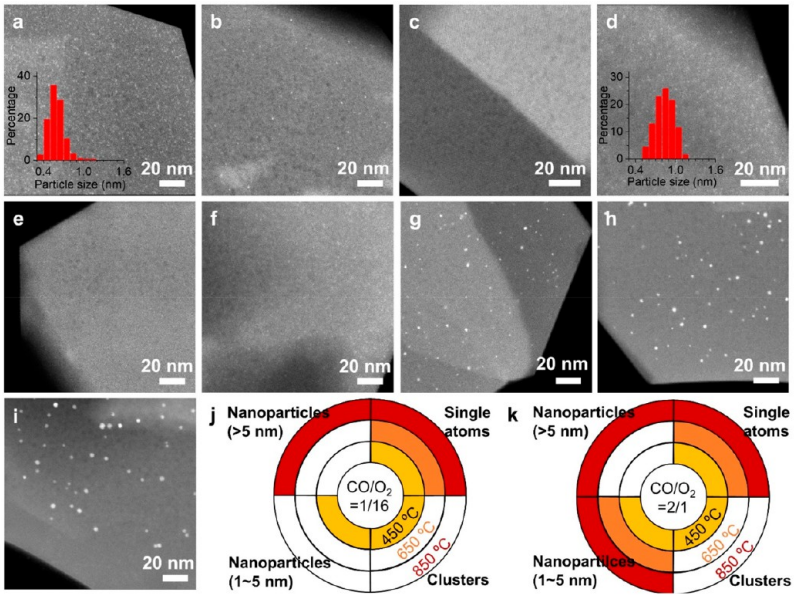

Figure 2. Structural characterization of Pt-MFI derived from treatments. Representative HAADF-STEM images are shown in this figure to show the morphological features of Pt-MFI samples obtained after different treatments. (a) Pt-MFI-fresh, (b) Pt-MFI-450-1/16, (c) Pt-MFI-650-1/16, (d) reduced Pt-MFI-650-1/16 sample by H_2 at 600 °C, (e) Pt-MFI-850-1/16, (f) reduced Pt-MFI-850-1/16 sample by H_2 at 600 °C, (g) Pt-MFI-450-2/1, (h) Pt-MFI-650-2/1, and (i) Pt-MFI-850-2/1. (j–k) General summary of the major compositions (in the form of single atoms, clusters, small nanoparticles (1–5 nm) or large nanoparticles (>5 nm)) of the Pt-MFI samples derived from treatments in a $CO+O_2$ atmosphere with different CO/O_2 ratios.

moisture is changed from N_2 to air, the sintering of Pt species is dramatically promoted, as inferred by the formation of Pt nanoparticles of (3–10 nm) after treatment at 450 °C (Figure S24) and the observation of very large Pt nanoparticles (>100 nm) in the field-emission scanning electron microscopy (FESEM) images after treatment at 650 °C (Figure S25), though some Pt species remain atomically dispersed in the MFI zeolite as suggested by the reversibly formed Pt clusters after reduction by H_2 (Figures S26 and S27). The aggravated sintering of Pt species in humid air (4% H_2O in air) can be ascribed to the formation of volatile PtO_x species in air and the diminishing of the anchoring sites for PtO_x species due to the structural deformation of MFI zeolite in moisture, as the defective sites comprise a large number of silanol groups according to the IR spectra (Figure S21c). Consequently, volatile PtO_x will migrate out of the MFI zeolite matrix and form thermodynamically bulky Pt/PtO_x particles.

By comparing the evolution behavior of Pt species in different atmospheres at 450–850 °C, we can find that the structural transformations are aggravated at higher temperatures because the interactions between Pt-MFI materials and the molecules (O_2, CO, and H_2O) are enhanced, especially in O_2 atmosphere. After all, the migration of volatile PtO_x species will be greatly promoted at >650 °C.

Evolution of Pt-MFI Catalyst in a $CO+O_2$ Reaction Atmosphere

The above results clearly show the atmosphere-dependent evolution of Pt species in MFI zeolite, which encourages us to further explore the structural transformation of Pt species in the reaction atmosphere. In the first case, we have studied the evolution of Pt species in the $CO+O_2$ atmosphere, which is a classic probe reaction for supported metal catalysts and model reaction in environmental catalysis.[25] After treatment in a $CO+O_2$ (CO/O_2 = 1/16) atmosphere at 450 °C (named as Pt-MFI-450-1/16), some of the initial Pt clusters (shown in Figure 2a) transform into small Pt nanoparticles accompanied by the redispersion of Pt nanoclusters into single atoms (Figure 2b and Figure S28), though a considerable amount of Pt clusters are also observed, whose location are the same as those in the fresh Pt-MFI sample according to the structural characterization results by HAADF-STEM and iDPC-STEM imaging technique[13,27] (Figure 3a–f). We would like to emphasize that the high-resolution HAADF-STEM and iDPC-STEM images were recorded under low-dose conditions (see the detailed description of imaging conditions in the experimental section) to minimize the influence of electron beam on the structure of the zeolite framework and the encapsulated Pt species.[27] The sintering of Pt species is possibly driven by CO, and is consistent with the structural evolution behavior of Pt atoms supported on metal oxides (i.e., Al_2O_3, TiO_2 and CeO_2).[13,17,32] The Pt nanoparticles are encapsulated in the MFI zeolite crystallite but may be located in defective regions in the zeolite matrix because their particle sizes exceed the pore dimensions of the 10MR channels of MFI zeolite, as inferred by the HAADF-STEM and paired iDPC-STEM images (Figure 3g, h). Consequently, the bimodal evolution behavior of Pt species in the CO/O_2(1/16) atmosphere at 450 °C suggests a competitive effect of CO and O_2. Increasing the treatment temperature to 650 °C causes a more remarkable redispersion behavior of Pt clusters than the scenario at 450 °C, as reflected by the significant diminishing of Pt clusters/nanoparticles in the HAADF-STEM images of Pt-MFI-650-1/16 sample (Figure 2c and Figure S29). The predominant presence of single Pt atoms in this sample is confirmed by high-resolution HAADF-STEM images (Figure 3i–l and Figure S30) and the IR measurements using CO as the probe molecule (Figure S31). Moreover, according to the HAADF-STEM and paired iDPC-STEM images, the single Pt atoms seem to be preferentially located in the 10MR sinusoidal channels of MFI zeolite, being similar to the location of the Pt

https://doi.org/10.1021/jacsau.3c00732
JACS Au 2024, 4, 666–679

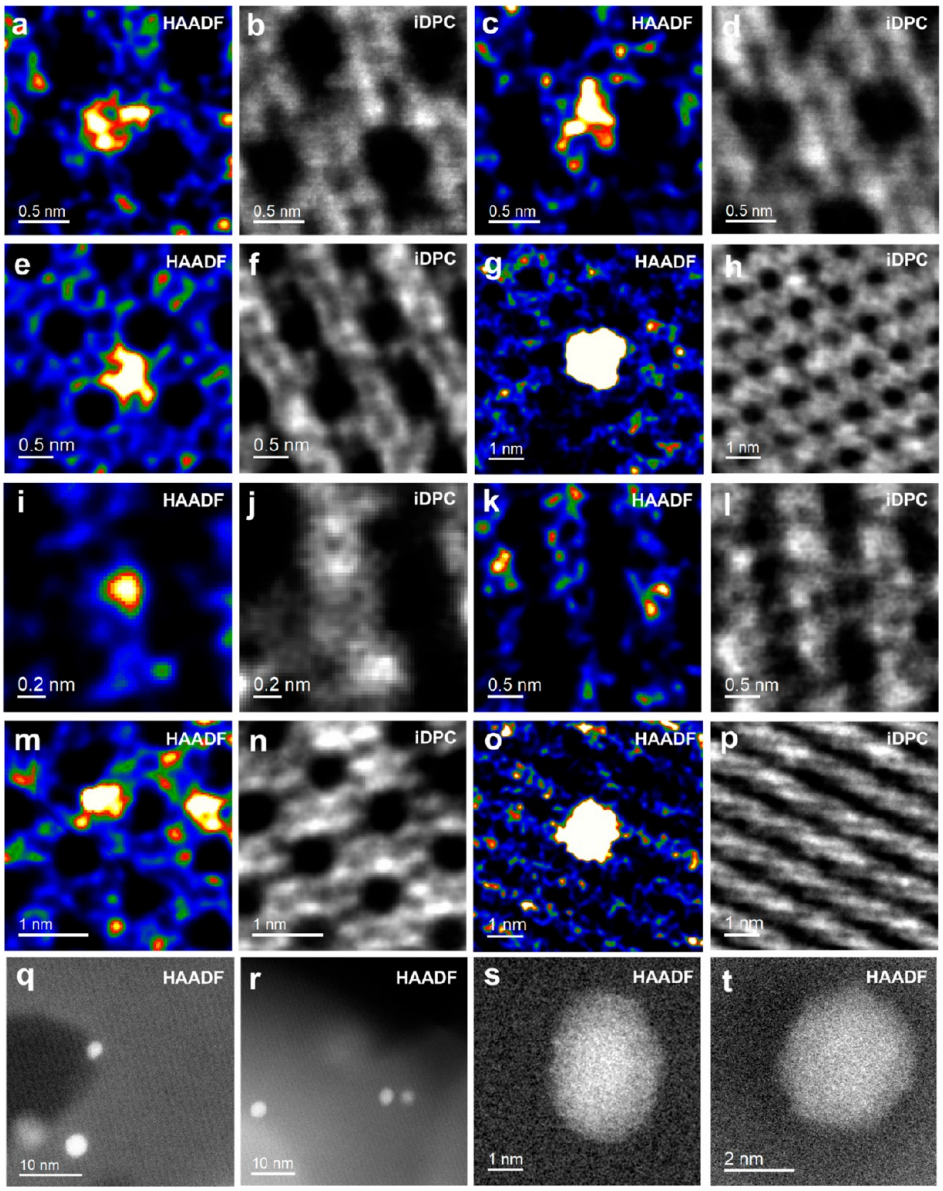

Figure 3. Characterization of Pt-MFI samples derived from different treatments by HAADF-STEM and iDPC-STEM imaging technique. (a–d) HAADF-STEM and the paired iDPC-STEM images of the fresh Pt-MFI sample, indicating the presence of subnanometer Pt clusters in the sinusoidal 10MR channels of MFI zeolite. (e–h) HAADF-STEM and the paired iDPC-STEM images of the Pt-MFI-450-1/16 sample, showing the presence of (e, f) subnanometer Pt clusters and (g, h) small Pt nanoparticles, respectively. (i–l) HAADF-STEM and the paired iDPC-STEM images of the Pt-MFI-650-1/16 sample, showing the presence of single Pt atoms within the 10MR channels of MFI zeolite. (m–p) HAADF-STEM and the paired iDPC-STEM images of the Pt-MFI-450-1/16-H_2O sample, showing the presence of (i, j) subnanometer Pt clusters and (k, l) small Pt nanoparticles, respectively. (q–t) HAADF-STEM images of the Pt-MFI-650-2/1-H_2O sample, showing the formation of Pt nanoparticles encapsulated in MFI zeolite. In panels q–t, the lattice fringes of the encapsulated Pt nanoparticles are absent due to the limited imaging depth under the working conditions.

clusters in the fresh Pt-MFI sample. Since the sintering of Pt particles occurs after the treatment with CO+N_2 atmosphere at 650 °C (Figure S13) and the redispersion of Pt clusters is observed after calcination in air at 650 °C (Figure S6), the evolution behavior of Pt species in CO/O_2(1/16) atmosphere at 650 °C is likely dictated by O_2. Subnanometer Pt clusters can also be recovered by reducing the Pt-MFI-650-1/16 sample with H_2 at 600 °C (Figure 2d and Figure S32), showing a reversible transformation of Pt species during the high-temperature treatments. When the treatment temperature is further elevated to 850 °C, redispersion of Pt species still happens in the Pt-MFI-850−1/16 sample (Figure 2e and Figures S33 and S34). However, a considerable portion of the Pt species sinter into very large Pt particles (>100 nm, as visualized in Figures S35 and S36 and Table S2), which should be ascribed to the migration and sintering of volatile PtO_x species at 850 °C.

By further comparing the Pt-MFI-650-1/16 and Pt-MFI-650-air samples, we can find that the addition of CO can partly suppress the O_2-induced sintering of Pt species at 650 °C, as supported by the Pt dispersion measured by CO-chemisorption (Table S2). With the CO/O_2 ratio further increased to 1/

https://doi.org/10.1021/jacsau.3c00732
JACS Au 2024, 4, 666–679

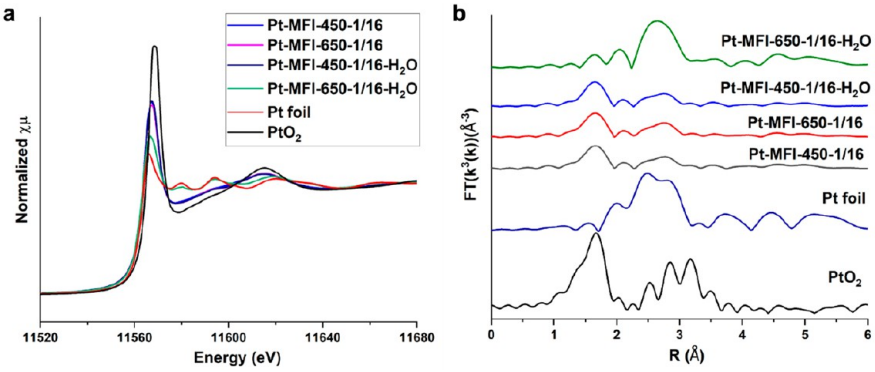

Figure 4. Characterization by X-ray absorption spectroscopy. (a) Pt-edge X-ray absorption near edge spectra and (b) Pt-edge extended X-ray absorption fine structure spectra of Pt-MFI samples and the reference Pt foil and PtO_2.

5, a much higher Pt dispersion is obtained, further confirming the suppressing effect of CO on the sintering of Pt. This effect can be attributed to the interconversion between PtO_x and $Pt(CO)_x$ because the diffusion of $Pt(CO)_x$ along the zeolite channels is more difficult than PtO_x due to its larger molecule size.[28] Considering the widely employed calcination treatments for regenerating Pt-based catalysts in industrial processes, the presence of an appropriate amount of CO in the oxidative atmosphere (usually air or diluted air) may facilitate to achieve a uniform redispersion of Pt species on the solid carrier.[37]

The results of X-ray absorption near edge spectroscopy (XANES) measurements indicate that the chemical states of Pt species in both Pt-MFI-450-1/16 and Pt-MFI-650-1/16 are close to the PtO_2 reference (Figure 4a). The extended X-ray adsorption fine structure (EXAFS) spectra show that both first-shell Pt−O and Pt−Pt bonds are present in the two samples (Figure 4b). The fitting results of both Pt-MFI-450-1/16 and Pt-MFI-650-1/16 samples are almost the same, giving coordination numbers of ∼4 and ∼2 for Pt−O and Pt−Pt bonding, respectively (Table 1). The XANES and EXAFS results further confirm the conclusions drawn from HAADF-STEM images that most Pt species are fragmented into single Pt atoms together with a few Pt clusters/nanoparticles, and the stabilized single Pt atoms are possibly coordinated to ∼4 oxygen atoms in zeolite. As inferred by the HAADF-STEM and FESEM images, the Pt-MFI-650-1/16 sample comprises more Pt nanoparticles than the Pt-MFI-450-1/16 sample, resulting in a slightly higher Pt−Pt coordination number.

Table 1. Fitting Results of the Pt-Edge EXAFS Spectra[a]

Sample	Path	R (Å)	CN	σ^2 (Å^2)	ΔE_0 (eV)	R-factor (%)
Pt-MFI-450-1/16	Pt−O	2.01(0)	3.5(1)	0.004(1)	13.5(11)	0.9
	Pt−Pt	2.78(1)	2.1(7)			
Pt-MFI-650-1/16	Pt−O	2.01(1)	3.9(1)	0.004(1)	12.9(16)	1.7
	Pt−Pt	2.79(1)	2.7(11)			
Pt-MFI-450-1/16-H_2O	Pt−O	2.00(1)	3.7(1)	0.003(1)	13.1(12)	1.1
	Pt−Pt	2.78(1)	2.3(8)			
Pt-MFI-650-1/16-H_2O	Pt−O	1.93(1)	1.3(1)	0.004(1)	7.6(6)	2.4
	Pt−Pt	2.78(1)	9.5(24)			

[a] S_0^2 was fixed as 0.83, which was obtained from Pt foil. Data range: 3.5 ≤ k ≤ 13 Å^{-1}, 1.3 ≤ R ≤ 3.1 Å. The number of variable parameters is 6, out of a total of 10.7 ($2\Delta k\Delta R/\pi$) independent data points.

In addition, we have then tracked the structural evolution of Pt species in a stoichiometric $CO+O_2$ mixture (CO/O_2 = 2/1) at 450−850 °C. It is obvious that the particle sizes of Pt particles formed in stoichiometric CO/O_2 atmosphere at 450 °C are slightly larger than those formed in $CO+O_2$ with excess O_2 (Figure 2g and Figure S37). When the treatment temperature is increased to 650−850 °C, many Pt nanoparticles are observed in the STEM images (Figure 2h, i and Figures S38 and S39), which are quite different to the disappearance of small Pt particles in the case of treatment with excess O_2. The redispersion of Pt clusters into atomically dispersed Pt species still occurs after treatments with stoichiometric $CO+O_2$, but in a less significant manner, as inferred by the reversibly formed Pt clusters after reduction by H_2 (Figures S40−S42). More importantly, the formation of large Pt particles (>20 nm) is greatly suppressed, as indicated by the electron microscopy images and XRD pattern of Pt-MFI-850-2/1 (Figures S43−S45), suggesting that the Pt species encapsulated in MFI zeolite remain highly stable in stoichiometric $CO+O_2$ mixture up to 850 °C.

Evolution of Pt-MFI Catalyst in a $CO+O_2+H_2O$ Atmosphere

The stability of metal species and zeolite under high-temperature treatments with moisture is a critical issue in terms of the practical applications of metal-zeolite catalysts.[38] Therefore, we have studied the structural transformation of Pt species encapsulated in MFI zeolite (Figure 5a) in a $CO+O_2+H_2O$ atmosphere. As shown in Figure 5b and 5g, in the case of treatments at 450 °C (with excess or stoichiometric O_2, named as Pt-MFI-450-1/16-H_2O and Pt-MFI-450−2/1-H_2O, respectively), small Pt nanoparticles with larger particle sizes are formed as observed with the Pt-MFI samples treated in a dry $CO+O_2$ atmosphere (Figures S46 and S47). The influence of moisture on the structural features of Pt-MFI in a $CO+O_2$ atmosphere at 450 °C is also reflected in the characterization results by the slightly increased Pt−Pt coordination number in the EXAFS fitting results (Table 1). At 450 °C, the introduction of H_2O should have a minor influence on the size distributions and location of Pt species. The locations of the Pt clusters and nanoparticles formed in the Pt-MFI-450-1/16-H_2O are quite similar to those formed in the Pt-MFI-450-1/16 sample, as suggested by the HAADF-STEM and iDPC-STEM images (Figure 3m−p).

As the temperature increased to 650 °C, remarkable changes in terms of the morphology of MFI zeolite crystallites and size

https://doi.org/10.1021/jacsau.3c00732
JACS Au 2024, 4, 666−679

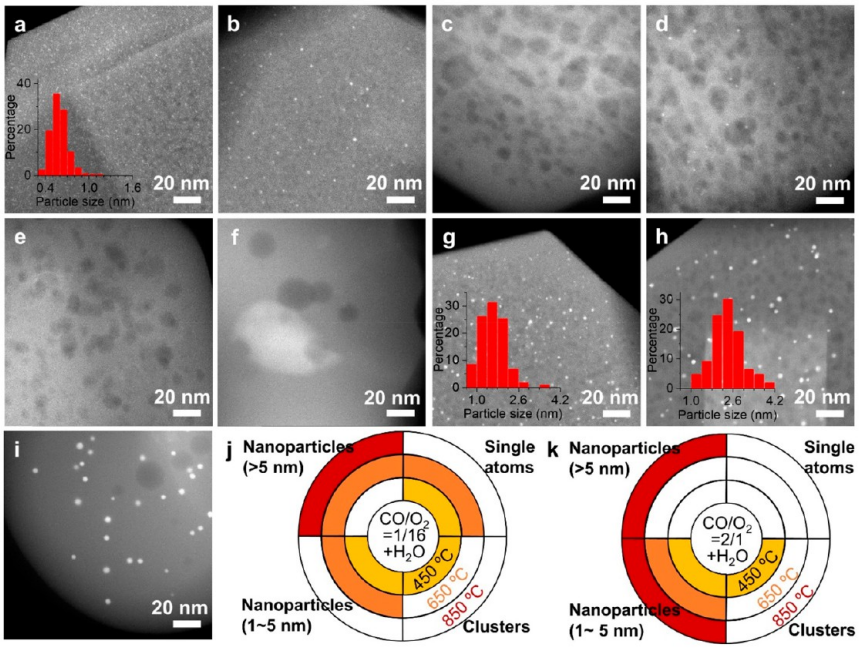

Figure 5. Structural characterization of Pt-MFI catalysts derived from treatments under moist conditions. HAADF-STEM images of the Pt-MFI samples for characterizing the size of Pt particles and the morphology of MFI zeolite. (a) Pt-MFI-fresh, (b) Pt-MFI-450-1/16-H_2O, (c) Pt-MFI-650-1/16-H_2O, (d) reduced Pt-MFI-650-1/16-H_2O sample by H_2 at 600 °C, (e) Pt-MFI-850-1/16-H_2O, (f) reduced Pt-MFI-850−1/16-H_2O sample by H_2 at 600 °C, (g) Pt-MFI-450−2/1-H_2O, (h) Pt-MFI-650-2/1-H_2O, and (i) Pt-MFI-850-2/1-H_2O. After high-temperature treatments (at 650 and 850 °C) under moist conditions, mesopores are formed in the MFI zeolite crystallites as defective sites. (j, k) General summary of the major compositions (in the form of single atoms, clusters, small nanoparticles (1−5 nm) or large nanoparticles (>5 nm)) of the Pt-MFI samples derived from treatments in a CO+O_2+H_2O atmosphere with different CO/O_2 ratios.

distributions of Pt particles are observed (Figure 5c and Figure S48). As marked in the HAADF-STEM images, mesopores are formed in the MFI zeolite crystallites due to the hydrolysis of Si−O−Si bonds during high-temperature treatments in the presence of moisture.[35,39] Only a few Pt clusters and small particles are found inside the MFI zeolite crystallites of the Pt-MFI-650-1/16-H_2O sample after reduction treatment by H_2 (Figure 5d and Figure S49). The white-line intensity of the XANES spectrum drops remarkably for the Pt-MFI-650-1/16-H_2O sample (Figure 4a), implying the predominant contribution of metallic Pt in this sample. The first-shell Pt−Pt coordination number of the Pt-MFI-650-1/16-H_2O sample increases to ∼9, corresponding to an average size of ∼2.5 nm,[40] accompanied by the decrease of Pt−O coordination number (Table 1). All of this information confirms the transformation of atomically dispersed Pt species to Pt particles, being consistent with the results from electron microscopy characterization.

XRD peaks associated with metallic Pt are observed in the Pt-MFI-650-1/16-H_2O sample, whose intensities are much stronger than that of the Pt-MFI-650-Air-H_2O sample, showing the enhanced agglomeration of Pt species with a CO+O_2+H_2O atmosphere (Figure S50). The migration of $Pt(CO)_x$ species formed in a CO atmosphere is facilitated due to the formation of mesopores in the MFI zeolite. Besides, the presence of a large number of disordered silanol groups in the MFI zeolite is not favorable for the anchoring of the $Pt(CO)_x$ species, which further accelerates the sintering of Pt species. Consequently, the interconversion from PtO_x to $Pt(CO)_x$ causes an aggravated sintering of Pt species in Pt-MFI-650-1/16-H_2O than the Pt-MFI-650-Air-H_2O sample.

In the case of Pt-MFI-650-2/1-H_2O, the sintering of Pt species into very large particles is greatly suppressed, though it gives broader size distribution and larger average particle size than the sample obtained under dry conditions (see Figure 5h and Figure S51), which could be associated with the deformation of the MFI zeolite structure and the higher mobility of $Pt(CO)_x$ species through the formed mesopores. The greatly suppressed agglomeration of large Pt particles is attributed to the enhanced conversion from PtO_x to $Pt(CO)_x$ and the lower mobility of $Pt(CO)_x$ than PtO_x. It should be noted that the Pt nanoparticles formed in the Pt-MFI-650-2/1-H_2O sample should probably be encapsulated within the MFI zeolite crystallites, as implied by the absence of lattice fringes in the high-resolution HAADF-STEM images, because of the limited imaging depth under our imaging conditions (Figure 3q−t). With the treatment of Pt-MFI at 850 °C under a moist atmosphere, the zeolite is transformed to cristobalite or amorphous SiO_2 as identified by XRD patterns (Figure S23). Due to the disruption of zeolite structure after hydrothermal treatment at 850 °C, severe sintering of Pt species happens regardless of the CO/O_2 ratio (see Figure 5e, 5i and Figures S52−S54).

As summarized in Figure 6, the Pt-MFI sample can undergo versatile transformations into Pt-zeolite materials with distinct structures depending on the treatment conditions. By employing suitable treatment conditions, we are able to tune the size of Pt species in a broad range, from single Pt atoms to Pt nanoparticles, which can serve as an effective approach for the generation of encapsulated metal particles with desired size distributions in zeolite structures. Notably, the conditions of the treatments could be different to those imposed for Pt-MFI catalysts, because the metal-reactant interaction, support-

https://doi.org/10.1021/jacsau.3c00732
JACS Au 2024, 4, 666−679

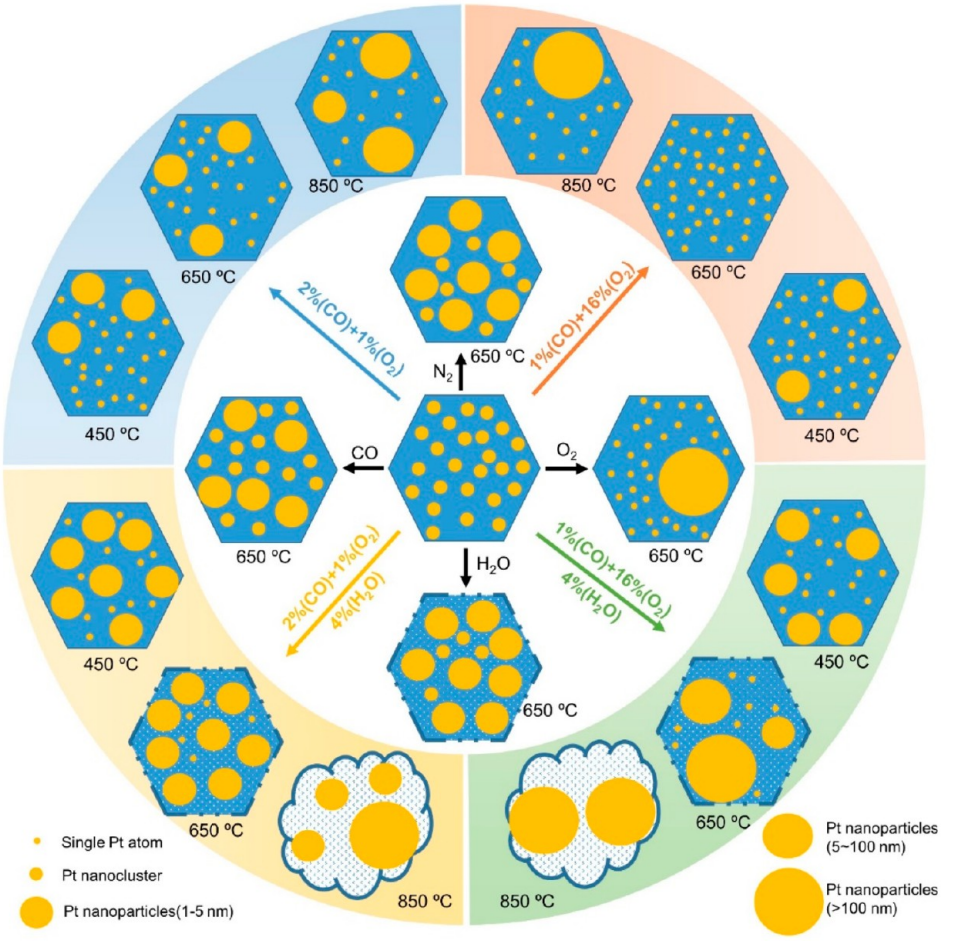

Figure 6. Dynamic evolution of Pt-MFI under different treatment conditions. The size distribution of the Pt species, the spatial distribution of the Pt species within the zeolite matrix and the morphology of the MFI zeolite support will be greatly dependent on the treatment atmosphere and temperature.

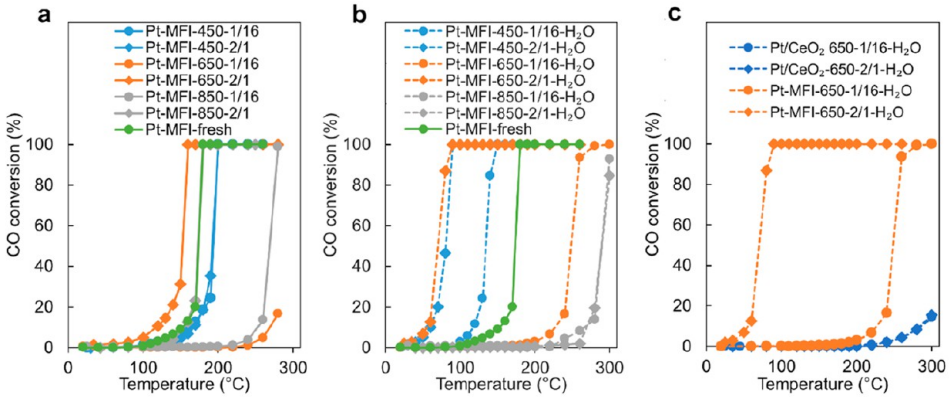

Figure 7. Catalytic performances of Pt-MFI and Pt/CeO_2 catalysts for CO oxidation reaction. (a) Pt-MFI catalysts derived from treatment under dry $CO+O_2$ atmosphere, (b) Pt-MFI catalysts derived from treatment under a moist $CO+O_2+H_2O$ atmosphere. (c) Catalytic performance of Pt/CeO_2 catalysts derived from treatment with $CO+O_2+H_2O$ at 650 °C.

reactant interaction and metal−support interaction can greatly affect the structural transformations of metal entities.[41−43]

Catalytic Performances of Pt-MFI Catalysts Derived from Different Treatments

With the various Pt-MFI samples comprising different types of Pt species in hand, we have attempted to study their catalytic performances for CO oxidation to establish the structure−reactivity relationship. As shown in Figure 7a, the pristine Pt-MFI sample requires a relatively high temperature (180 °C) to achieve full conversion of CO. The Pt-MFI samples obtained after treatments with a $CO+O_2$ atmosphere, regardless of the CO/O_2 ratio, show similar activity or even worse performances than the pristine Pt-MFI sample, except for Pt-MFI-650-2/1. In particular, the Pt-MFI-650-1/16 sample containing

https://doi.org/10.1021/jacsau.3c00732
JACS Au 2024, 4, 666−679

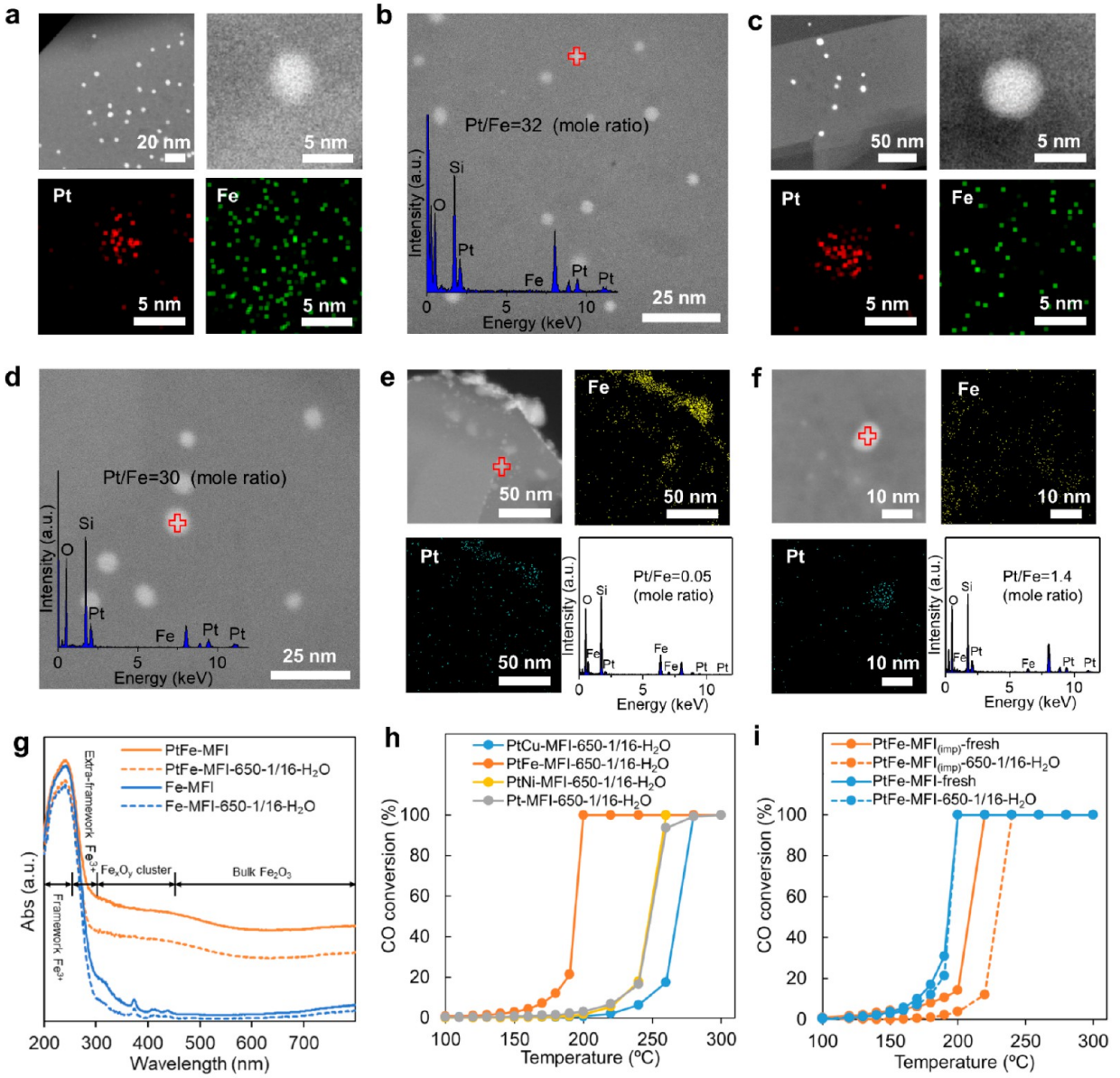

Figure 8. Bimetallic PtM-MFI catalysts derived from treatments under moist conditions. (a, b) HAADF-STEM images of PtFe-MFI-fresh sample, EDS mapping, and point analysis of the Pt particles. (c, d) HAADF-STEM images of PtFe-MFI-650-1/16-H_2O sample, EDS mapping, and point analysis of the Pt particles. (e, f) HAADF-STEM images, EDS mapping, and point analysis of (e) PtFe/$MFI_{(imp)}$-fresh and (f) PtFe/$MFI_{(imp)}$-650-1/16-H_2O. (g) UV−vis spectra of PtFe-MFI and Fe-MFI samples. The bands at 200−250, 250−300, 300−450, and >450 nm correspond to tetrahedral coordinated framework Fe^{3+}, isolated extra-framework Fe^{3+} cations, FeOx clusters and bulk FeOx, respectively. (h, i) Catalytic performances of PtM-MFI samples (h) and PtFe/$MFI_{(imp)}$ samples (i) derived from treatments in CO+O_2+H_2O atmosphere (1%CO, 16% O_2 and 4%H_2O (balanced by N_2)) at 650 °C.

predominantly single Pt atoms exhibits quite poor activity. Moreover, Pt clusters and Pt particles are formed in the Pt-MFI-650-1/16 sample after the CO oxidation test (Figure S55). These results imply that single Pt atoms exhibit low catalytic activity as well as low stability under CO oxidation condition.

The catalytic performances of the Pt-MFI catalysts obtained from treatments under humid conditions are shown in Figure 7b. Some of the treatments with a moist CO+O_2 (CO/O_2 = 1/16) atmosphere will cause significant deactivation of Pt-MFI catalysts, especially at high temperatures (650 and 850 °C), which are consistent with the severe sintering of Pt species into large particles. However, moisture exhibits a more positive effect on the reactivity when the Pt-MFI samples are treated with a stochiometric CO+O_2 (CO/O_2 = 2/1) atmosphere. As shown in Figure 7b, remarkable shifts of the T50 (temperature for achieving 50% CO conversion) to much lower temperatures are observed after treatments at 450−650 °C. Moreover, the stability of the Pt nanoparticles generated by treatments in a CO+O_2+H_2O (CO/O_2 = 2/1) atmosphere has been tested for the CO oxidation reaction in a cyclic manner. As presented in Figure S56, the Pt-MFI-650-2/1-H_2O sample shows almost the same behavior in three consecutive tests, and the size distributions of Pt particles are preserved in the used catalyst (Figure S57). The excellent stability of the Pt-MFI-650-2/1-

https://doi.org/10.1021/jacsau.3c00732
JACS Au 2024, 4, 666−679

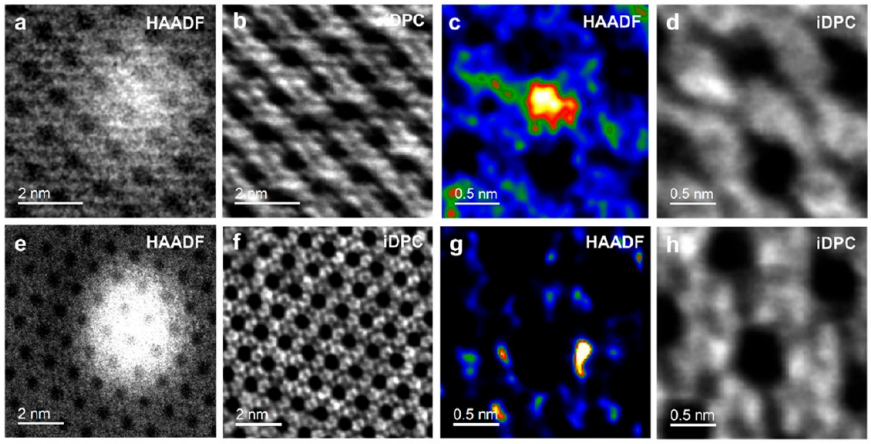

Figure 9. Characterization of the fresh PtFe-MFI and PtFe-MFI-650-1/16-H_2O sample by HAADF-STEM and iDPC-STEM imaging technique. (a–d) HAADF-STEM and the paired iDPC-STEM images of fresh PtFe-MFI sample, which indicate (a, b) the presence of a Pt nanoparticle encapsulated in MFI zeolite and (c, d) the presence of subnanometer Pt clusters in the sinusoidal channels of MFI zeolite, respectively. (e–h) HAADF-STEM and the paired iDPC-STEM images of PtFe-MFI-650-1/16-H_2O sample, which indicate (e, f) the presence of a Pt nanoparticle encapsulated in MFI zeolite and (g, h) the presence of single Pt atoms in the sinusoidal channels of MFI zeolite, respectively. In panels a and e, the lattice fringes of the encapsulated Pt nanoparticles are absent due to the limited imaging depth under the working conditions.

H_2O sample is also validated by the long-term test for ∼24 h at 85 °C (Figure S58 and S59).

Pt/CeO_2 has been reported as a reference catalyst with high stability against sintering because of the strong Pt-CeO_2 interaction. In this work, taking a Pt/CeO_2 prepared according to literature works as a reference material, we have tested the stability of Pt species upon exposure to different treatments. As shown in Figure S60, the agglomeration of Pt is not observed with Pt/CeO_2 sample, because the strong metal–support interaction between Pt and CeO_2 is in favor of trapping mobile PtO_x as single Pt atoms.[44,45] Though the isolated Pt atoms stabilized by CeO_2 are resistant to sintering, they show poor activity for CO oxidation (Figure 7c), which is consistent with the reported works.[7] The comparison between Pt/CeO_2 and Pt-MFI materials shows that Pt nanoparticles with suitable sizes encapsulated in a zeolite matrix can be a promising candidate for the removal of CO under harsh reaction conditions.

Structure–Reactivity Correlation in Pt-MFI Catalysts

Based on the characterization and reactivity information on various Pt-MFI catalysts, we have attempted to correlate their structural features and catalytic performances. Pt species are categorized into four types depending on the size distribution of Pt species from STEM images: single Pt atoms, subnanometer Pt clusters, small Pt particles (1–5 nm) and large Pt nanoparticles (>5 nm). By correlating the information in Figure 6 and Figure 7, we can show that the Pt-MFI catalysts with superior performance mainly comprise Pt particles with moderate sizes (1–5 nm), as shown with the Pt-MFI samples derived from treatment with stochiometric $CO+O_2$ atmospheres. The single Pt atoms exhibit very low activities for CO oxidation and may evolve into Pt clusters/nanoparticles under reaction conditions. In the case of subnanometer Pt clusters and large Pt nanoparticles (>5 nm), they show moderate activity for CO oxidation. We have also calculated the intrinsic activities of the Pt species in several representative Pt-zeolite catalysts predominantly made of Pt nanoparticles by normalizing the reaction rates at 60 °C to the exposed Pt sites measured by CO chemisorption. As listed in Table S3, for the three Pt-MFI samples treated with a dry stoichiometric $CO+O_2$ atmosphere, the highest activity achieved with the Pt-MFI-650-2/1 sample could be associated with the appropriate particle size in this sample. For the two Pt-MFI samples treated with a moist $CO+O_2$ atmosphere, both samples exhibit one-order magnitude higher TOFs than the samples obtained in a dry $CO+O_2$ atmosphere, which is in line with the catalytic results presented in the light-off curves shown in Figure 7.

We further tracked the activities of representative Pt catalysts during the heating and cooling cycles (Figure S61), which could reflect the structural evolution of various Pt entities under reaction conditions. For Pt-MFI-650-2/1-H_2O and Pt-MFI-650-1/16-H_2O, the activity in the cooling process is consistent with that of the heating process. However, for Pt-MFI-fresh, Pt-MFI-650-1/16, and Pt-MFI-650-2/1, the activities at the cooling processes are slightly enhanced than those obtained at the heating processes. The particle sizes of the small Pt nanoparticles in the Pt-MFI-650-2/1-H_2O and Pt-MFI-650-1/16-H_2O almost remain unchanged, which could be relevant to the passivation effect of the hydrothermal treatment (Figures S62 and S63). The enhanced activity of fresh Pt-MFI should be ascribed to the agglomeration of Pt clusters to small Pt particles (Figure S64), while the improved activities of Pt-MFI-650-1/16 and Pt-MFI-650-2/1 are attributed to the transformation of redispersed single Pt atoms to small Pt particles during the heating process (Figure S65 and S66). These results further confirm that the small Pt particles are the most active species and the encapsulation of Pt nanoparticles with appropriate sizes in zeolite matrix can generate highly active and stable catalyst for CO oxidation, being consistent with the superior performances of Pt ensembles observed in supported Pt-based catalysts.[7,46,47]

Evolution and Catalytic Consequence of Bimetallic PtM-MFI Catalyst

Incorporating 3d metals into Pt particles to form bimetallic catalysts has been demonstrated as an efficient strategy to enhance the catalytic performance for CO oxidation and the thermal stability of Pt species.[48,49] Harsh treatments ($CO+O_2+H_2O$ mixture with a CO/O_2 ratio of 1/16) at 650 °C are chosen as the conditions to test the stability of the bimetallic

https://doi.org/10.1021/jacsau.3c00732
JACS Au 2024, 4, 666–679

PtM-MFI materials prepared by a one-pot synthesis. Some Pt particles are present in the fresh PtCu-MFI and PtFe-MFI (Figure S67 and S68 and Figure 8a) but the PtNi-MFI sample shows a similar morphology as the Pt-MFI (Figure S69), indicating the type of 3d metal will affect the dispersion of Pt species during the one-pot synthesis.[50] The paired HAADF-STEM and iDPC-STEM images show that Pt clusters are located in the sinusoidal channels of MFI zeolite, while the Pt nanoparticles are encapsulated within the MFI zeolite crystallites (Figure 9a–d). After high-temperature treatments, severe sintering of Pt species into very large Pt particles is observed with the bimetallic PtNi and PtCu samples after treatment at 650 °C, while a large number of small Pt nanoparticles (1–10 nm) are formed in the PtFe-MFI-650-1/16-H_2O sample (see Figures S70–S72 and Figure 8c), suggesting that the incorporation of Fe species can effectively protect the Pt nanoparticles from severe sintering. High-resolution HAADF-STEM images show that the Pt nanoparticles formed in the PtFe-MFI-650-1/16-H_2O sample are still encapsulated within the MFI zeolite crystallites, as implied by the difficulty in obtaining the lattice fringes in the high-resolution HAADF-STEM images.

EDS analysis results show that the Pt nanoparticles in the fresh PtFe-MFI and PtFe-MFI-650-1/16-H_2O sample contain very low amounts of Fe (with Pt/Fe ratios >30, as shown in Figure 8b, Figure 8d and Figures S73 and S74). The EDS mappings of the fresh and treated samples show that the Pt nanoparticles are surrounded by some Fe species (Figure 8a, c). According to the UV–vis spectra (Figure 8g), the majority of the Fe species is likely atomically dispersed in the MFI zeolite structure, either at the framework positions or at extra-framework positions.[51−53] The Fe(III) species at the framework positions will cause the formation of negatively charged zeolite framework sites, which can serve as the anchoring sites for the PtO_x species at high temperatures, as reported in the Al(III) species in ZSM-5 zeolite for stabilization of PtO_x.[54] The extra framework Fe(III) species in PtFe-MFI possibly provide new sites for the anchoring of mobile PtO_x via the formation of Pt–O–Fe bond in the moist oxidative atmosphere, as observed with supported Pt/FeO_x catalysts and the Pt atoms supported on model Fe_3O_4 surface.[55−57] Indeed, in the PtFe-MFI-650-1/16-H_2O sample, we observed the presence of single Pt atoms located in the sinusoidal channels according to the HAADF-STEM and paired iDPC-STEM images (Figure 9g–h).

The Pt species in the PtFe-MFI-650-1/16-H_2O sample exhibit higher stability than those in the Pt-MFI-650-1/16-H_2O sample, as reflected in the presence of more Pt nanoparticles in the PtFe-MFI-650-1/16-H_2O sample (Figure S75). Higher Pt dispersion measured by CO chemisorption (Table S2) and less intensive Pt(111) diffraction peak in the XRD pattern (Figure S76) further confirm the alleviated agglomeration of Pt species in PtFe-MFI-650-1/16-H_2O. The discrepancy in the abundance of Pt nanoparticles of 1–10 nm could cause their difference in catalytic activity for the CO oxidation reaction because the small Pt nanoparticles are more active than the large ones.[58] As shown in Figure 8h, The PtFe-MFI-650-1/16-H_2O sample exhibits much better performances than the Pt-MFI and bimetallic PtCu and PtNi samples. As shown in Table S4, the PtFe-MFI sample prepared in this work exhibits performance superior to that of the supported Pt catalysts derived from hydrothermal treatments under comparative conditions.

The necessity of the simultaneous encapsulation of Fe and Pt species into zeolite crystallites for the generation of highly stable Pt nanoparticles against sintering is validated by the control experiments with the PtFe/$MFI_{(imp)}$ sample prepared by impregnating Pt and Fe precursors on MFI. FeO_x aggregates are formed on the external surface of MFI zeolite crystallites in PtFe/$MFI_{(imp)}$ and Pt nanoparticles are in contact with the FeO_x patches on the external surface of MFI zeolite crystallites. Such Pt-FeO_x structures are less efficient for the stabilization of the Pt species in comparison to the highly dispersed Fe sites within the MFI zeolite structure (Figure 8e and Figure S77). Severe sintering of Pt into large nanoparticles is observed in the PtFe/$MFI_{(imp)}$-650-1/16-H_2O sample after harsh hydrothermal treatment (Figure 8f and Figure S78). Consequently, the PtFe/$MFI_{(imp)}$ sample prepared by impregnation exhibits much lower activity for the CO oxidation reaction than the PtFe-MFI prepared by one-pot synthesis (Figure 8i). The lower stability against sintering of the PtFe/$MFI_{(imp)}$ sample is also confirmed by the declined activity of the PtFe/$MFI_{(imp)}$-650-1/16-H_2O sample.

CONCLUSIONS

In summary, by treating the Pt-MFI materials under various conditions, we can modulate the size distributions of Pt species encapsulated in the zeolite matrix from single Pt sites to Pt nanoparticles. Size-controllable Pt nanoparticles (1–5 nm) are stabilized in the zeolite matrix with resistance to sintering up to 650 °C in the presence of a CO+O_2+H_2O atmosphere. The stable Fe–O–Pt bonding interaction can further promote the stability of Pt species under harsh treatments, leading to the formation of highly active and stable catalysts for CO oxidation. The lessons learned with Pt-MFI can be translated to other metal-zeolite catalysts for tuning the particle sizes in confined space and then facilitating the formation and stabilization of active sites for the target reactions.

Besides the CO oxidation reaction, we anticipate that the structural evolution of supported single metal atoms may occur in other catalytic reactions, especially in the presence of reductive atmospheres.[13,59] The identification of the working active sites and discrimination of the contribution of different types of metal species require rigorous and comprehensive characterizations of the composition of supported metal catalysts and systematic monitoring of the structural features of the catalysts along the reaction process. Moreover, comparative studies based on a series of catalysts with variations in particle size distributions will also help to clarify the predominant active sites in a specific reaction.

EXPERIMENTAL SECTION

Catalyst Preparation

One-Pot Synthesis of Pt-MFI. Pt nanocluster well encapsulated in MFI zeolite was prepared via one-pot synthesis. 16.24 g of tetrapropylammonium hydroxide (TPAOH, 1M, ThermoFisher) was mixed with 12 g of deionized water and 8.24 g of tetraethyl orthosilicate (TEOS, 99+%, ThermoFisher). At the same time, 0.07 g of KCl (99.5%, SINOPHARM) was added to the mixture. After 9 h of stirring, the above solution was separated into two equal parts. Then, 150 μL H_2PtCl_6 solution (0.19 mol/L Pt) and 150 μL ethylenediamine (99%, ThermoFisher) were added into each part of the above solution with 20 min stirring. Finally, the resultant solution was transferred into Teflon-lined autoclaves

https://doi.org/10.1021/jacsau.3c00732
JACS Au 2024, 4, 666–679

and heated in the oven at 175 °C for 4 days. The hydrothermal synthesis product was washed twice with deionized water and acetone and separated via centrifugation. After dried at 60 °C, the solid sample was calcined in muffle furnace at 560 °C for 8 h in air with a heating rate of 2 °C/min from room temperature to 560 °C. After natural cooling to room temperature, the sample was further calcined at 600 °C for 2 h in air with a heating rate of 5 °C/min from room temperature to 600 °C. Hereafter, the calcined sample would be transferred to a quartz tube furnace and further reduced by 5%H_2 (balanced by Ar) at 600 °C for 2 h, giving to the formation of the Pt-MFI-Fresh sample. It should be noted that the additional KCl in the synthesis mixture is to stabilize the subnanometer Pt species within the MFI zeolite channels from sintering during the postsynthesis treatments.

One-Pot Synthesis of PtM-MFI (M = Cu, Fe, Ni). The procedure for the synthesis of PtM-containing MFI zeolite was similar to that of Pt-MFI. The difference is that, before the addition of H_2PtCl_6 and ethylenediamine, 19 mg $CuCl_2$ (98%, MERYER) or 58 mg $Fe(NO_3)_3{\cdot}9H_2O$ (99.9%, Macklin) or 36 mg $NiC_4H_6O_4{\cdot}4H_2O$ (98%, SINOPHARM) was doped into the hydrolysis solution, and kept stirring for 30 min at room temperature. Then, H_2PtCl_6 and ethylenediamine were added to the mixture, and the rest of the procedures were the same as that for the preparation of the Pt-MFI sample.

Fe-MFI reference sample was also prepared in a procedure similar to Pt-MFI. After 9 h of stirring of the mixture of TPAOH, TEOS, and KCl, 58 mg of $Fe(NO_3)_3{\cdot}9H_2O$ (99.9%, Macklin) was added into the mixture, followed by stirring for 20 min. Then, 150 μL of ethylenediamine (99%, Thermo-Fisher) was added to the above solution followed by stirring for 30 min. Afterward, the resultant solution was transferred into Teflon-lined autoclaves and heated in the oven at 175 °C for 4 days. The treatments after the hydrothermal synthesis (sample washing, separation, calcination, and reduction procedures) were the same as that of the synthesis of Pt-MFI sample.

Synthesis of Pt/CeO_2 Catalysts. Nanosized CeO_2 (99.9%, 50 nm, Macklin) was chosen for the preparation of reference Pt/CeO_2 catalyst by wetness impregnation. Two g of the CeO_2 powder was dispersed in 20 mL of deionized water under stirring. Then, 210 μL of H_2PtCl_6 solution (0.19 mol/L) was added to the above suspension, and the mixture was kept stirring for 6 h. After that, the mixture was dried at 60 °C. The resultant solid sample would be calcined at 560 °C for 8 h, and then at 600 °C for 2 h in air. The calcined sample was further reduced by 5% H_2 (balanced by Ar) at 600 °C for 2 h.

Preparation of Pt/Al_2O_3 and Pt-Free MFI Mixture. Nanosized Al_2O_3 (99.99%, γ phase, 40 nm, Meryer) was chosen as the support for the preparation of Pt/Al_2O_3 catalyst. Two g of Al_2O_3 powder and 210 μL of H_2PtCl_6 solution (0.19 mol/L Pt) were added into 20 mL of deionized water, and the mixture was kept stirring for 6 h. After that, the mixture was dried at 60 °C, and calcined at 560 °C for 8 h and at 600 °C for 2 h in air. The calcined sample would be further reduced by 5% H_2 (balanced by Ar) at 600 °C for 2 h. Pt-free MFI zeolite was prepared similar to that of Pt-MFI zeolite; the only difference is that H_2PtCl_6 and ethylenediamine are excluded in the batch composition for hydrothermal synthesis. The Pt/Al_2O_3 and Pt-free MFI powder were physically mixed with a mass ratio of 1/1 before further post-treatment.

Treatment of Pt Supported Catalyst under Various Conditions

The as-prepared Pt-MFI, PtM-MFI, and Pt/CeO_2 catalysts were pelleted to 40−60 mesh and loaded in a quartz tube furnace with 500 mg of catalyst grain for further post-treatments. Different atmosphere (N_2, air, 4% H_2O (balanced by N_2 or air) and 1%CO (balanced by N_2)) were used in the treatments. Moreover, mixed gases such as 1%CO-16%O_2-4% H_2O(when applicable)-N_2 or 2%CO-1%O_2-4%H_2O(when applicable)-N_2 were all applied for the high-temperature treatments of the supported Pt catalyst. The flow rate was controlled to be 100 mL/min in all the treatments. The treatment temperature was set to be 450, 650, or 850 °C with a ramp rate of 5 °C/min, respectively and the treatment lasted for 6 h at each temperature. After the treatment, the system would be cooled to room temperature and the solid sample was recovered for characterizations or catalytic tests.

Characterization

X-ray powder diffraction was conducted on a Bruker AXS D8 ADVANCE with Cu Kα radiation, working at 40 mA and 40 kV and scanning in the 2-theta range of 5−50°.

Samples for electron microscopy studies were prepared by dropping the suspension of the solid samples in CH_2Cl_2 directly onto holey-carbon-coated copper grids. Electron microscopy measurements were performed using two types of microscopes. Thus, noncorrected JEOL 2100F microscope operating at 200 kV both in transmission (TEM) and scanning-transmission modes (STEM) was used to record High Angle Annular Dark Field (HAADF), Z-contrast, images at low resolution. High-resolution HAADF-STEM and STEM-iDPC imaging was performed on a double aberration corrected (AC), monochromated, FEI Titan^3 Themis 60−300 microscope working at 300 kV. The last technique, iDPC (integrated-Differential Phase Contrast) imaging, provides in this microscope atomically resolved images in which the contrasts are related to the atomic number of the elements under the beam, instead of the roughly Z^2-dependent contrasts obtained in HAADF-STEM images. By using a 4-segment detector, this technique allows imaging light elements (such as Si and O) under low-dose conditions to avoid the beam damage to zeolite structure. In particular, 2048 × 2048 HAADF-iDPC image pairs were recorded simultaneously. This configuration allowed us to optimize the collection of the signals on the HAADF and FEI DF4 detectors. In order to mitigate the damage by the electron beam, a fast image recording protocol was used by combining a beam current of 10−30 pA, a 2.5 μs dwell time, and an automated fine-tuning alignment of A1 and C1 using the OptiSTEM software. To obtain images with good quality, the beam current and image acquisition time should be optimized according to the stability of the sample under the beam.

Infrared (IR) spectra of the silanol groups in the Pt-zeolite samples were measured by a Bruker V70 instrument equipped with a liquid nitrogen-cooled HgCdTe detector. Transmission IR studies were conducted with self-supporting wafers (14−16 mg cm^{-2}) of catalyst materials. For IR measurements, the samples underwent pretreatment at 400 °C at a pressure of 10^{-3} Pa for 1 h, followed by the acquisition of IR spectra after cooling to room temperature. Diffuse Reflectance Infrared Fourier Transform Spectroscopy (DRIFTS) using CO as the probe molecule was employed to probe the presence of positively charged Pt atoms in the Pt-zeolite samples. The

https://doi.org/10.1021/jacsau.3c00732
JACS Au 2024, 4, 666−679

CO−DRIFTS experiments were performed with an in situ IR cell (PIKE, DIFFUSIRTM). Before measurements, the sample was subjected to pretreatment with helium flow at 100 °C for 1 h and then cooled to room temperature in a helium flow. Subsequently, the sample was exposed to CO (5 vol % balanced with helium) for 10 min, and IR spectra were recorded after purging gaseous CO with helium flow.

CO pulse chemisorption was conducted on an automatic chemisorption analyzer (BSD-Chem C200) to determine the dispersion of Pt species in Pt supported samples. The samples (100−200 mg) would be pretreated under H_2 atmosphere at 600 °C for 2h, and then cooled to the adsorption temperature at 50 °C. After purging with He, CO pulses were injected for several times until the cumulative quantity of adsorbed CO reached saturation. The quantity adsorbed of each CO pulse was recorded by a thermal conductivity detector, and the metal dispersion was calculated as assuming that the ratio of surface Pt/adsorbed CO was 1.

Ar isotherm adsorption was conducted on a BSD-660 M A6M surface area and aperture analyzer, and the isotherm adsorption of Ar was performed at 87.3 K. Degas of the catalyst sample was performed in vacuum at 200 °C for 3 h to eliminate the influence of adsorbed impurities. H−K methods were used to calculate the aperture size distribution.

UV−vis was conducted on an Agilent Cary5000 to point out the position of Fe species in PtFe-MFI zeolite at a photometric range of 200−800 nm. Powders were loaded in sample carrier with quartz glass window, and the baseline was recorded via $BaSO_4$.

Performance of CO Oxidation

For each testing, 50 mg of catalyst sample (40−60 mesh) was physically mixed with 500 mg of quartz sand (40−60 mesh) and loaded in a quartz tube with 6 mm internal diameter. Our control experiments indicate that the catalytic tests are performed in the absence of heat and mass transport limitations. The inlet gas consisted of 1% CO and 16% O_2, with the balance being N_2. The outlet gas was measured via gas chromatography (GC990, Agilent). The CO oxidation activity was tested from room temperature to 300 °C. At each temperature point, the outlet concentration of CO ($CO_{(outlet)}$) was recorded until the concentration of CO has kept unchanged for 10 min. The conversion of CO oxidation was calculated via the following equation.

$$\text{CO conversion} = \frac{1 - CO_{(outlet)}}{CO_{(inlet)}}$$

■ ASSOCIATED CONTENT

Supporting Information

The Supporting Information is available free of charge at https://pubs.acs.org/doi/10.1021/jacsau.3c00732.

Chemical compositions of the metal-zeolite materials, electron microscopy and spectroscopy results of the metal-zeolite materials, results of catalytic tests, characterizations of the spent catalysts, and summary of the catalytic performances reported in the literature (PDF)

■ AUTHOR INFORMATION

Corresponding Authors

Huaming Hou − *National Energy Center for Coal to Clean Fuels, Synfuels China Co., Ltd., Huairou District, Beijing 101407, China*; Email: houhuaming@synfuelschina.com.cn

Lichen Liu − *Engineering Research Center of Advanced Rare Earth Materials, Department of Chemistry, Tsinghua University, Beijing 100084, China*; orcid.org/0000-0001-5067-0481; Email: lichenliu@mail.tsinghua.edu.cn

Authors

Xiaoyu Li − *Engineering Research Center of Advanced Rare Earth Materials, Department of Chemistry, Tsinghua University, Beijing 100084, China*

Jinling Cheng − *Engineering Research Center of Advanced Rare Earth Materials, Department of Chemistry, Tsinghua University, Beijing 100084, China;* Present Address: Institute of Analysis and Testing, Beijing Academy of Science and Technology, Beijing 100089, China

Debora M. Meira − *CLS@APS sector 20, Advanced Photon Source, Argonne National Laboratory, Argonne, Illinois 60439, United States; Canadian Light Source Inc., Saskatoon, Saskatchewan S7N 2 V3, Canada;* orcid.org/0000-0002-7529-2736

Complete contact information is available at: https://pubs.acs.org/10.1021/jacsau.3c00732

Author Contributions

†X.L. and J.C. contributed equally. CRediT: **Xiaoyu Li** data curation, formal analysis, investigation, writing-original draft, writing-review & editing; **Jinling Cheng** data curation, formal analysis, investigation; **Huaming Hou** data curation, formal analysis, investigation; **Debora Motta Meira** data curation, investigation; **Lichen Liu** conceptualization, data curation, formal analysis, funding acquisition, investigation, methodology, project administration, resources, writing-original draft, writing-review & editing.

Notes

The authors declare no competing financial interest.

■ ACKNOWLEDGMENTS

L.L. acknowledges the financial supports from the National Natural Science Foundation of China (22272087), Tsinghua University (Initiative Scientific Research Program (20233080016), International Joint Mission on Climate Change and Carbon Neutrality (20233080033) and Dushi Program (20231080010)), and SINOPEC Corporation. This research used resources of the Advanced Photon Source, an Office of Science User Facility operated for the U.S. Department of Energy (DOE) Office of Science by Argonne National Laboratory, and was supported by the U.S. DOE under Contract No. DE-AC02-06CH11357, and the Canadian Light Source and its funding partners.

■ REFERENCES

(1) Liu, L.; Corma, A. Metal Catalysts for Heterogeneous Catalysis: From Single Atoms to Nanoclusters and Nanoparticles. *Chem. Rev.* **2018**, *118* (10), 4981−5079.

(2) Li, Z.; Ji, S.; Liu, Y.; Cao, X.; Tian, S.; Chen, Y.; Niu, Z.; Li, Y. Well-Defined Materials for Heterogeneous Catalysis: From Nanoparticles to Isolated Single-Atom Sites. *Chem. Rev.* **2020**, *120* (2), 623−682.

(3) Liu, L.; Corma, A. Evolution of Isolated Atoms and Clusters in Catalysis. *Trends Chem.* **2020**, *2* (4), 383−400.

(4) Liu, L.; Corma, A. Structural transformations of solid electrocatalysts and photocatalysts. *Nat. Rev. Chem.* **2021**, *5* (4), 256−276.
(5) Wan, G.; Zhang, G.; Chen, J. Z.; Toney, M. F.; Miller, J. T.; Tassone, C. J. Reaction-Mediated Transformation of Working Catalysts. *ACS Catal.* **2022**, *12* (13), 8007−8018.
(6) Krishna, S. H.; Jones, C. B.; Gounder, R. Dynamic Interconversion of Metal Active Site Ensembles in Zeolite Catalysis. *Annu. Rev. Chem. Biomol. Eng.* **2021**, *12*, 115−136.
(7) Maurer, F.; Jelic, J.; Wang, J.; Gänzler, A.; Dolcet, P.; Wöll, C.; Wang, Y.; Studt, F.; Casapu, M.; Grunwaldt, J.-D. Tracking the formation, fate and consequence for catalytic activity of Pt single sites on CeO_2. *Nat. Catal.* **2020**, *3* (10), 824−833.
(8) Resasco, J.; Christopher, P. Atomically Dispersed Pt-group Catalysts: Reactivity, Uniformity, Structural Evolution, and Paths to Increased Functionality. *J. Phys. Chem. Lett.* **2020**, *11* (23), 10114−10123.
(9) Resasco, J.; DeRita, L.; Dai, S.; Chada, J. P.; Xu, M.; Yan, X.; Finzel, J.; Hanukovich, S.; Hoffman, A. S.; Graham, G. W.; et al. Uniformity Is Key in Defining Structure-Function Relationships for Atomically Dispersed Metal Catalysts: The Case of Pt/CeO_2. *J. Am. Chem. Soc.* **2020**, *142* (1), 169−184.
(10) Corma, A.; Concepcion, P.; Boronat, M.; Sabater, M. J.; Navas, J.; Yacaman, M. J.; Larios, E.; Posadas, A.; Lopez-Quintela, M. A.; Buceta, D.; et al. Exceptional oxidation activity with size-controlled supported gold clusters of low atomicity. *Nat. Chem.* **2013**, *5* (9), 775−781.
(11) Nelson, N. C.; Chen, L.; Meira, D.; Kovarik, L.; Szanyi, J. In Situ Dispersion of Palladium on TiO2 During Reverse Water-Gas Shift Reaction: Formation of Atomically Dispersed Palladium. *Angew. Chem., Int. Ed.* **2020**, *132* (40), 17810−17816.
(12) Albrahim, M. A.; Shrotri, A.; Unocic, R. R.; Hoffman, A. S.; Bare, S. R.; Karim, A. M. Size Dependent Dispersion of Rhodium Clusters into Isolated Single Atoms at Low Temperature and the Consequences for CO Oxidation Activity. *Angew. Chem., Int. Ed.* **2023**, *62* (44), e202308002.
(13) Liu, L.; Meira, D. M.; Arenal, R.; Concepcion, P.; Puga, A. V.; Corma, A. Determination of the Evolution of Heterogeneous Single Metal Atoms and Nanoclusters under Reaction Conditions: Which Are the Working Catalytic Sites? *ACS Catal.* **2019**, *9* (12), 10626−10639.
(14) Resasco, J.; Dai, S.; Graham, G.; Pan, X.; Christopher, P. Combining In-Situ Transmission Electron Microscopy and Infrared Spectroscopy for Understanding Dynamic and Atomic-Scale Features of Supported Metal Catalysts. *J. Phys. Chem. C* **2018**, *122* (44), 25143−25157.
(15) Bayram, E.; Lu, J.; Aydin, C.; Browning, N. D.; Özkar, S.; Finney, E.; Gates, B. C.; Finke, R. G. Agglomerative Sintering of an Atomically Dispersed Ir_1/Zeolite Y Catalyst: Compelling Evidence Against Ostwald Ripening but for Bimolecular and Autocatalytic Agglomeration Catalyst Sintering Steps. *ACS Catal.* **2015**, *5* (6), 3514−3527.
(16) Mehrabadi, B. A. T.; Eskandari, S.; Khan, U.; White, R. D.; Regalbuto, J. R. A Review of Preparation Methods for Supported Metal Catalysts. *Adv. Catal.* **2017**, *61*, 1−35.
(17) Dessal, C.; Len, T.; Morfin, F.; Rousset, J.-L.; Aouine, M.; Afanasiev, P.; Piccolo, L. Dynamics of Single Pt Atoms on Alumina during CO Oxidation Monitored by Operando X-ray and Infrared Spectroscopies. *ACS Catal.* **2019**, *9* (6), 5752−5759.
(18) Serna, P.; Rodríguez Fernández, A.; Yacob, S.; Kliewer, C.; Moliner, M.; Corma, A. Single Site vs. Cluster Catalysis in High Temperature Oxidations. *Angew. Chem., Int. Ed.* **2021**, *133* (29), 16090−16098.
(19) Moliner, M.; Gabay, J. E.; Kliewer, C. E.; Carr, R. T.; Guzman, J.; Casty, G. L.; Serna, P.; Corma, A. Reversible Transformation of Pt Nanoparticles into Single Atoms inside High-Silica Chabazite Zeolite. *J. Am. Chem. Soc.* **2016**, *138* (48), 15743−15750.
(20) Dessal, C.; Sangnier, A.; Chizallet, C.; Dujardin, C.; Morfin, F.; Rousset, J.-L.; Aouine, M.; Bugnet, M.; Afanasiev, P.; Piccolo, L. Atmosphere-dependent stability and mobility of catalytic Pt single atoms and clusters on γ-Al_2O_3. *Nanoscale* **2019**, *11* (14), 6897−6904.
(21) Shin, S.; Haaring, R.; So, J.; Choi, Y.; Lee, H. Highly Durable Heterogeneous Atomic Catalysts. *Acc. Chem. Res.* **2022**, *55* (10), 1372−1382.
(22) Xiong, H.; Pham, H. N.; Datye, A. K. Hydrothermally stable heterogeneous catalysts for conversion of biorenewables. *Green Chem.* **2014**, *16* (11), 4627−4643.
(23) Murata, K.; Ohyama, J.; Yamamoto, Y.; Arai, S.; Satsuma, A. Methane Combustion over Pd/Al2O3 Catalysts in the Presence of Water: Effects of Pd Particle Size and Alumina Crystalline Phase. *ACS Catal.* **2020**, *10* (15), 8149−8156.
(24) van Spronsen, M. A.; Frenken, J. W. M.; Groot, I. M. N. Surface science under reaction conditions: CO oxidation on Pt and Pd model catalysts. *Chem. Soc. Rev.* **2017**, *46* (14), 4347−4374.
(25) Freund, H. J.; Meijer, G.; Scheffler, M.; Schlögl, R.; Wolf, M. CO Oxidation as a Prototypical Reaction for Heterogeneous Processes. *Angew. Chem., Int. Ed.* **2011**, *50* (43), 10064−10094.
(26) Liu, L.; Lopez-Haro, M.; Lopes, C. W.; Rojas-Buzo, S.; Concepcion, P.; Manzorro, R.; Simonelli, L.; Sattler, A.; Serna, P.; Calvino, J. J.; et al. Structural modulation and direct measurement of subnanometric bimetallic PtSn clusters confined in zeolites. *Nat. Catal.* **2020**, *3* (8), 628−638.
(27) Liu, L.; Lopez-Haro, M.; Calvino, J. J.; Corma, A. Tutorial: structural characterization of isolated metal atoms and subnanometric metal clusters in zeolites. *Nat. Protoc.* **2021**, *16* (4), 1871−1906.
(28) Felvey, N.; Guo, J.; Rana, R.; Xu, L.; Bare, S. R.; Gates, B. C.; Katz, A.; Kulkarni, A. R.; Runnebaum, R. C.; Kronawitter, C. X. Interconversion of Atomically Dispersed Platinum Cations and Platinum Clusters in Zeolite ZSM-5 and Formation of Platinum gem-Dicarbonyls. *J. Am. Chem. Soc.* **2022**, *144* (30), 13874−13887.
(29) Burton, A.; Terefenko, E.; Wang, H.; Paccagnini, M.; Sattler, A. Structure-property relationships that influence platinum stability in all-silica or highly siliceous zeolites. *Microporous Mesoporous Mater.* **2023**, *358*, 112411.
(30) Moliner, M.; Gabay, J. E.; Kliewer, C. E.; Carr, R. T.; Guzman, J.; Casty, G. L.; Serna, P.; Corma, A. Reversible Transformation of Pt Nanoparticles into Single Atoms inside High-Silica Chabazite Zeolite. *J. Am. Chem. Soc.* **2016**, *138* (48), 15743−15750.
(31) Ding, K.; Gulec, A.; Johnson, A. M.; Schweitzer, N. M.; Stucky, G. D.; Marks, L. D.; Stair, P. C. Identification of active sites in CO oxidation and water-gas shift over supported Pt catalysts. *Science* **2015**, *350* (6257), 189−192.
(32) Bliem, R.; van der Hoeven, J. E.; Hulva, J.; Pavelec, J.; Gamba, O.; de Jongh, P. E.; Schmid, M.; Blaha, P.; Diebold, U.; Parkinson, G. S. Dual role of CO in the stability of subnano Pt clusters at the Fe3O4(001) surface. *Proc. Natl. Acad. Sci. U.S.A.* **2016**, *113* (32), 8921−8926.
(33) Ogel, E.; Casapu, M.; Doronkin, D. E.; Popescu, R.; Störmer, H.; Mechler, C.; Marzun, G.; Barcikowski, S.; Türk, M.; Grunwaldt, J. D. Impact of Preparation Method and Hydrothermal Aging on Particle Size Distribution of Pt/γ-Al_2O_3 and Its Performance in CO and NO Oxidation. *J. Phys. Chem. C* **2019**, *123* (9), 5433−5446.
(34) Datye, A. K.; Votsmeier, M. Opportunities and challenges in the development of advanced materials for emission control catalysts. *Nat. Mater.* **2021**, *20* (8), 1049−1059.
(35) Zhang, L.; Chen, K.; Chen, B.; White, J. L.; Resasco, D. E. Factors that Determine Zeolite Stability in Hot Liquid Water. *J. Am. Chem. Soc.* **2015**, *137* (36), 11810−11819.
(36) Ravenelle, R. M.; Schüßler, F.; D'Amico, A.; Danilina, N.; van Bokhoven, J. A.; Lercher, J. A.; Jones, C. W.; Sievers, C. Stability of Zeolites in Hot Liquid Water. *J. Phys. Chem. C* **2010**, *114* (46), 19582−19595.
(37) Alcala, R.; Dean, D. P.; Chavan, I.; Chang, C.-W.; Burnside, B.; Pham, H. N.; Peterson, E.; Miller, J. T.; Datye, A. K. Strategies for regeneration of Pt-alloy catalysts supported on silica for propane dehydrogenation. *Appl. Catal. A: Gen.* **2023**, *658*, 119157.
(38) Simancas, R.; Chokkalingam, A.; Elangovan, S. P.; Liu, Z.; Sano, T.; Iyoki, K.; Wakihara, T.; Okubo, T. Recent progress in the

improvement of hydrothermal stability of zeolites. *Chem. Sci.* **2021**, *12* (22), 7677−7695.
(39) Jin, M.; Liu, M.; Nachtigall, P.; Grajciar, L.; Heard, C. J. Mechanism of Zeolite Hydrolysis under Basic Conditions. *Chem. Mater.* **2021**, *33* (23), 9202−9212.
(40) Jentys, A. Estimation of mean size and shape of small metal particles by EXAFS. *Phys. Chem. Chem. Phys.* **1999**, *1* (17), 4059−4063.
(41) Liu, A.; Liu, L.; Cao, Y.; Wang, J.; Si, R.; Gao, F.; Dong, L. Controlling Dynamic Structural Transformation of Atomically Dispersed CuOx Species and Influence on Their Catalytic Performances. *ACS Catal.* **2019**, *9* (11), 9840−9851.
(42) Wei, S.; Li, A.; Liu, J. C.; Li, Z.; Chen, W.; Gong, Y.; Zhang, Q.; Cheong, W. C.; Wang, Y.; Zheng, L.; et al. Direct observation of noble metal nanoparticles transforming to thermally stable single atoms. *Nat. Nanotechnol.* **2018**, *13* (9), 856−861.
(43) Huang, Z.; Ban, T.; Zhang, Y.; Wang, L.; Guo, S.; Chang, C.-R.; Jing, G. Boosting the thermal stability and catalytic performance by confining Ag single atom sites over antimony-doped tin oxide via atom trapping. *Appl. Catal. B: Environ.* **2021**, *283*, 119625.
(44) Pereira-Hernandez, X. I.; DeLaRiva, A.; Muravev, V.; Kunwar, D.; Xiong, H.; Sudduth, B.; Engelhard, M.; Kovarik, L.; Hensen, E. J. M.; Wang, Y.; Datye, A. K. Tuning Pt-CeO_2 interactions by high-temperature vapor-phase synthesis for improved reducibility of lattice oxygen. *Nat. Commun.* **2019**, *10* (1), 1358.
(45) Nie, L.; Mei, D.; Xiong, H.; Peng, B.; Ren, Z.; Hernandez, X. I. P.; DeLaRiva, A.; Wang, M.; Engelhard, M. H.; Kovarik, L.; et al. Activation of surface lattice oxygen in single-atom Pt/CeO_2 for low-temperature CO oxidation. *Science* **2017**, *358* (6369), 1419−1423.
(46) Jeong, H.; Kwon, O.; Kim, B.-S.; Bae, J.; Shin, S.; Kim, H.-E.; Kim, J.; Lee, H. Highly durable metal ensemble catalysts with full dispersion for automotive applications beyond single-atom catalysts. *Nat. Catal.* **2020**, *3* (4), 368−375.
(47) Pereira-Hernandez, X. I.; DeLaRiva, A.; Muravev, V.; Kunwar, D.; Xiong, H.; Sudduth, B.; Engelhard, M.; Kovarik, L.; Hensen, E. J. M.; Wang, Y.; Datye, A. K. Tuning Pt-CeO_2 interactions by high-temperature vapor-phase synthesis for improved reducibility of lattice oxygen. *Nat. Commun.* **2019**, *10* (1), 1358.
(48) Fu, Q.; Li, W. X.; Yao, Y.; Liu, H.; Su, H. Y.; Ma, D.; Gu, X. K.; Chen, L.; Wang, Z.; Zhang, H.; et al. Interface-confined ferrous centers for catalytic oxidation. *Science* **2010**, *328* (5982), 1141−1144.
(49) Chen, G.; Zhao, Y.; Fu, G.; Duchesne, P. N.; Gu, L.; Zheng, Y.; Weng, X.; Chen, M.; Zhang, P.; Pao, C. W.; et al. Interfacial effects in iron-nickel hydroxide-platinum nanoparticles enhance catalytic oxidation. *Science* **2014**, *344* (6183), 495−499.
(50) Prats, H.; Alonso, G.; Sayós, R.; Gamallo, P. Transition metal atoms encapsulated within microporous Silicalite-1 zeolite: A systematic computational study. *Microporous Mesoporous Mater.* **2020**, *308*, 110462.
(51) Guo, D.; Shen, B.; Qin, Y.; Sun, J.; Guo, Q.; Ren, S.; Gao, X.; Pang, X.; Wang, B.; Zhao, H.; Liu, H. USY zeolites with tunable mesoporosity designed by controlling framework Fe content and their catalytic cracking properties. *Microporous Mesoporous Mater.* **2015**, *211*, 192−199.
(52) Agote-Arán, M.; Lezcano-González, I.; Greenaway, A. G.; Hayama, S.; Díaz-Moreno, S.; Kroner, A. B.; Beale, A. M. Operando HERFD-XANES/XES studies reveal differences in the activity of Fe-species in MFI and CHA structures for the standard selective catalytic reduction of NO with NH_3. *Appl. Catal. A: Gen.* **2019**, *570*, 283−291.
(53) Zeng, J.; Wang, Y.; Diao, F.; Qiu, L.; Chang, H. Selective Catalytic Reduction of N_2O by CO over Fe-Beta Zeolites Catalysts: Influence of Iron Species Distribution. *Catal. Surveys Asia* **2021**, *25* (1), 58−67.
(54) Felvey, N.; Guo, J.; Rana, R.; Xu, L.; Bare, S. R.; Gates, B. C.; Katz, A.; Kulkarni, A. R.; Runnebaum, R. C.; Kronawitter, C. X. Interconversion of Atomically Dispersed Platinum Cations and Platinum Clusters in Zeolite ZSM-5 and Formation of Platinum gem-Dicarbonyls. *J. Am. Chem. Soc.* **2022**, *144* (30), 13874−13887.
(55) Bordiga, S.; Buzzoni, R.; Geobaldo, F.; Lamberti, C.; Giamello, E.; Zecchina, A.; Leofanti, G.; Petrini, G.; Tozzola, G.; Vlaic, G. Structure and Reactivity of Framework and Extraframework Iron in Fe-Silicalite as Investigated by Spectroscopic and Physicochemical Methods. *J. Catal.* **1996**, *158* (2), 486−501.
(56) Zhang, J.; Tang, X.; Yi, H.; Yu, Q.; Zhang, Y.; Wei, J.; Yuan, Y. Synthesis, characterization and application of Fe-zeolite: A review. *Appl. Catal. A: Gen.* **2022**, *630*, 118467.
(57) Bliem, R.; van der Hoeven, J. E. S.; Hulva, J.; Pavelec, J.; Gamba, O.; de Jongh, P. E.; Schmid, M.; Blaha, P.; Diebold, U.; Parkinson, G. S. Dual role of CO in the stability of subnano Pt clusters at the Fe_3O_4(001) surface. *Proc. Natl. Acad. Sci. U.S.A.* **2016**, *113* (32), 8921−8926.
(58) Liu, A.; Liu, X.; Liu, L.; Pu, Y.; Guo, K.; Tan, W.; Gao, S.; Luo, Y.; Yu, S.; Si, R.; et al. Getting Insights into the Temperature-Specific Active Sites on Platinum Nanoparticles for CO Oxidation: A Combined in Situ Spectroscopic and ab Initio Density Functional Theory Study. *ACS Catal.* **2019**, *9* (9), 7759−7768.
(59) Resasco, J.; Yang, F.; Mou, T.; Wang, B.; Christopher, P.; Resasco, D. E. Relationship between Atomic Scale Structure and Reactivity of Pt Catalysts: Hydrodeoxygenation of m-Cresol over Isolated Pt Cations and Clusters. *ACS Catal.* **2020**, *10* (1), 595−603.

https://doi.org/10.1021/jacsau.3c00732
JACS Au 2024, 4, 666−679